Temperature-compensated fiber optic Fabry-Perot accelerometer based on the feedback control of the Fabry-Perot cavity length

Pinggang Jia (贾平岗)[1,2] and Daihua Wang (王代华)[1,2*]

[1]*Key Laboratory of Optoelectronic Technology and Systems of the Ministry of Education of China, Chongqing University, Chongqing 400044, China*

[2]*Precision and Intelligence Laboratory, Department of Optoelectronic Engineering, Chongqing University, Chongqing 400044, China*

[*]*Corresponding author: dhwang@cqu.edu.cn*

Received September 14, 2012; accepted December 7, 2012; posted online March 6, 2013

A temperature-compensated fiber optic Fabry-Perot accelerometer (FOFPA) formed by symmetrically bonding an all-silica in-line fiber Fabry-Perot etalon (ILFFPE) and a piezoelectric ceramic unimorph actuator (PCUA) to two surfaces of a silica cantilever is reported. The all-silica ILFFPE with feedback-controlled cavity length by the PCUA simultaneously senses acceleration and temperature. The results indicate that the fabricated FOFPA system simultaneously senses acceleration and temperature with active temperature compensation. The nonlinearity of the output voltage to acceleration is less than 0.65%. The nonlinearity of the control voltage to temperature is 1.75%. Furthermore, the maximum deviation of the sensitivity with temperature compensation at a temperature range from 25 to 50 °C is 0.025 V/g.

OCIS codes: 060.2370, 060.5060, 120.3180, 120.2230.

doi: 10.3788/COL201311.040601.

In the past three decades, various fiber optic accelerometers (FOAs) based on different principles have been developed. Based on modulation methods, FOAs can be mainly categorized into intensity modulation type[1], wavelength modulation type[2−7], and phase modulation type[8−19]. Phase modulation type FOAs have attracted considerable interest because of their high performance and low cost. The commonly used configurations for fiber optic interferometric accelerometers include Mach-Zehnder interferometers[8], Michelson interferometers[9−15], and Fabry-Perot interferometers[16−19]. Fabry-Perot interferometers are extremely sensitive to perturbations that affect the optical path length between two reflectors. Furthermore, the sensor head of fiber optic Fabry-Perot accelerometers contain no fiber couplers, resulting in a very compact sensing structure.

Several types of Fabry-Perot cavities based on different principles, such as fiber Bragg grating/long-period fiber grating Fabry-Perot cavities or in-line fiber Fabry-Perot etalons (ILFFPEs), have been proposed[18−25]. The all-silica ILFFPEs are fabricated by splicing a section of hollow fiber, hollow-core photonic crystal, or silica capillary tube to two single-mode fibers (SMFs)[18,19,23−25]. Small ILFFPEs can be easily fabricated and can be used to measure stress, pressure, ultrasound, acceleration, and other parameters[18,19,23−25]. Corres *et al.*[18] proposed an ILFFPE-based accelerometer in which the inertial mass was suspended by a fiber parallel to a rubber band for vibration monitoring of electrical engines. The pretensioning rubber band is used to set the operating point of the accelerometer at the quadrature point. However, the large cross-sensitivity makes the accelerometer sensitive to acceleration in any direction. Ke *et al.*[19] developed an all-fiber Fabry-Perot accelerometer by gluing a fiber optic Fabry-Perot cavity on a uniform cantilever. The Fabry-Perot cavity was formed by splicing the ends of two SMFs to the cleaved end of a hollow-core photonic crystal fiber. The initial phases of the two above-mentioned fiber optic Fabry-Perot interferometric accelerometers are biased at the quadrature point to measure vibration. Although sensor systems based on phase-biased demodulation possess high resolution, wide frequency bandwidth, and simple structure, the phase bias point is very sensitive to environmental perturbations and needs to be stabilized[26−29]. Considering that the phase bias point of fiber optic Fabry-Perot interferometric accelerometers is very sensitive to the thermal expansion of ILFFPEs and spring elements, thermal variations may cause a huge error or distortion in the desired results if temperature compensation is not achieved.

In this letter, the principle of a temperature-compensated fiber optic Fabry-Perot accelerometer (FOFPA) formed by symmetrically bonding an ILFFPE and a piezoelectric ceramic unimorph actuator (PCUA) to two surfaces of a silica cantilever is described and analyzed. A FOFPA prototype system and an experimental setup are established, and the sensing characteristics of the FOFPA system are tested and analyzed.

Figures 1(a) and (b) show the structural configuration and photograph of the temperature-compensated FOFPA based on an all-silica ILFFPE. Figure 2 shows the schematic of the FOFPA system with active temperature compensation. Figure 1(a) shows that the all-silica ILFFPE is formed by fusing a short section of a silica capillary tube with an outer diameter of 125 μm and an inner diameter of 50 μm between the ends of two optical fibers (type: SMF-28e). The all-silica ILFFPE and PCUA were symmetrically bonded to two surfaces of a silica cantilever (length: 25 mm, width: 20 mm, and thickness: 1 mm) with a lumped mass at the free

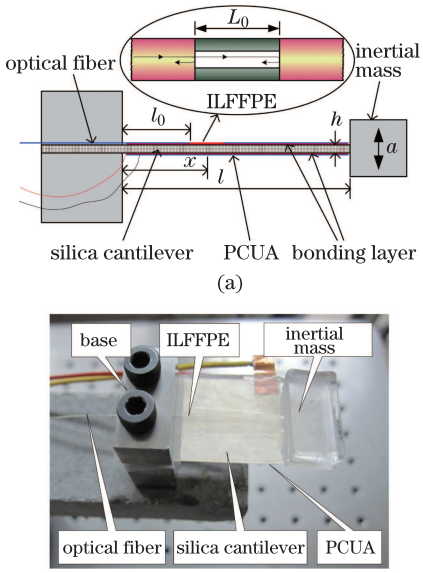

Fig. 1. FOFPA based on an all-silica ILFFPE with collocated PCUA. (a) Structural configuration and (b) photograph.

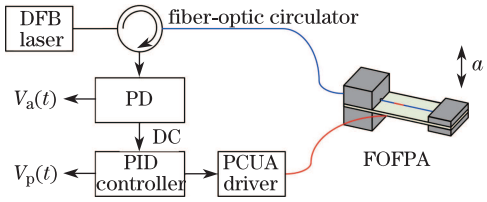

Fig. 2. Schematic of the FOFPA system with active temperature compensation.

end. The silica cantilever with a lumped mass at the free end acts as a mass–spring–damper system for translating the inertial force of the inertial mass into the cavity length change of the all-silica ILFFPE. As shown in Fig. 2, when the light from a distributed feedback (DFB) laser is impinged on the FOFPA via a fiber optic circulator, the phase shifts of the interference output from the FOFPA are directly proportional to the cavity length change of the all-silica ILFFPE. The acceleration can then be obtained by demodulating the phase shifts. The collocated PCUA can be used to control the cavity length of the all-silica ILFFPE for active temperature compensation. To compensate for the thermal strain of the all-silica ILFFPE, the cavity length of the all-silica ILFFPE is feedback controlled by the PCUA using the proportional–integral–derivative (PID) algorithm. Considering that the control voltage applied to the PCUA is proportional to temperature, acceleration and temperature can be simultaneously measured.

As shown in Fig. 1, when on-axis acceleration excitation is applied to the FOFPA, the inertial force ($F(t)$) of the inertial mass and strain ($\varepsilon_x(t)$) of the silica cantilever with a lumped mass at the free end can be expressed as

$$F(t) = ma(t), \tag{1}$$

$$\varepsilon_x(t) = \frac{6(l-x)}{Ebh^2} F(t), \tag{2}$$

where m is the equivalent mass of the inertial mass; $a(t)$ is the acceleration applied on the inertial mass; l, b, and h are the length, width, and thickness, respectively, of the silica cantilever; E is the elastic modulus of the silica cantilever; x is the position of the point on the cantilever from the clamped end.

Based on Eq. (2), the strain of the silica cantilever is not uniform, and the strain of the all-silica ILFFPE attached on the cantilever is related to the position from the clamped end. The length change ($L_a(t)$) of the all-silica ILFFPE can be expressed as

$$L_a(t) = \int_{l_0}^{l_0+L_0} \frac{6\eta m a(t)}{Ebh^2}(l-x)\,\mathrm{d}x = \frac{6\eta m a(t)}{Ebh^2}\left(lL_0 - \frac{1}{2}L_0^2 - l_0L_0\right), \tag{3}$$

where l_0 is the position from the clamped end, L_0 is the cavity length of the all-silica ILFFPE, and η ($\leqslant 1$) is the strain transfer coefficient between the cantilever and all-silica ILFFPE.

The phase shifts ($\phi_a(t)$) of the interference output from the FOFPA generated by acceleration excitation can be expressed as

$$\phi_a(t) = \frac{4\pi n}{\lambda} L_a(t), \tag{4}$$

where $L_a(t)$ is the length change of the all-silica ILFFPE generated by the acceleration excitation, n is the refractive index, and λ is the wavelength of the DFB laser.

Based on Eqs. (1) to (4), the relationship between the phase shifts of the interference output from the FOFPA and measured acceleration can be expressed as

$$\phi_a(t) = K_a a(t), \tag{5}$$

where K_a is the phase sensitivity and can be expressed as

$$K_a = \frac{24\pi nm\eta\left(lL_0 - \frac{1}{2}L_0^2 - l_0L_0\right)}{\lambda Ebh^2}. \tag{6}$$

Based on Eqs. (5) and (6), the phase shifts ($\phi_a(t)$) of the interference output from the FOFPA are proportional to the measured acceleration ($a(t)$), and the acceleration can be accessed by demodulating the phase shifts. Figure 3 shows the demodulation scheme of the FOFPA. The initial phase is adjusted to maintain the operating point at point Q when no acceleration excitation is applied to the FOFPA. When on-axis acceleration excitation is applied to the FOFPA, the corresponding points of the phase shifts are marked as A and B. Considering the small phase shifts ($\phi_a(t)$), the intensity change between A and B can be considered as linear. Thus, the intensity change of the interference output can be regarded as proportional to the phase shifts of the interference output. Based on the intensity change of the interference output by a photodetector (PD), the voltage output can be expressed as

$$V_a(t) = C\beta R + K_a K_Q \beta R a(t), \tag{7}$$

where C is the corresponding laser intensity of the quadrature point Q, β is the fraction of the laser intensity

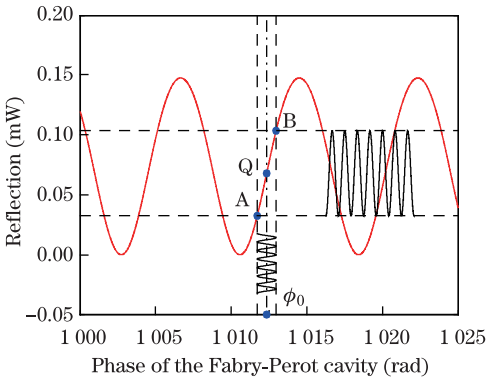

Fig. 3. Demodulation scheme of the FOFPA.

from the FOFPA directed to the PD, R is the response factor of the PD, and K_{Q} is the slope at the quadrature point Q.

The thermal strain of the all-silica ILFFPE caused by the temperature variation of the FOFPA can change the bias point. The cavity length variation of the all-silica ILFFPE produced by the PCUA can also change the bias point. Active temperature compensation can be achieved when the bias point of the all-silica ILFFPE is maintained through the active feedback control of the cavity length by the PCUA. Figure 2 shows that the control voltage, which is generated by the PID controller and amplified by the PCUA driver, is applied to the PCUA to maintain a constant direct current (DC) of the measured acceleration for active temperature compensation.

The thermal strain ($L_{\mathrm{e}}(t)$) and length change ($L_{\mathrm{p}}(t)$) of the all-silica ILFFPE produced by the PCUA can be expressed as

$$L_{\mathrm{e}}(t) = \kappa_1 T(t) L_0, \tag{8}$$

$$L_{\mathrm{p}}(t) = -\kappa_2 V_{\mathrm{p}}(t), \tag{9}$$

where κ_1 is the coefficient of the thermal expansion of the silica capillary, $T(t)$ is the temperature change, κ_2 is the cavity length change of the all-silica ILFFPE per unit voltage, and $V_{\mathrm{p}}(t)$ is the control voltage applied to the PCUA.

Considering that the wavelength (λ) of the DFB laser and the refractive index (n) are constant when the operating temperature of the FOFPA is changed, the PCUA can offset the thermal strain of the all-silica ILFFPE by changing the cavity length to achieve the temperature compensation of the FOFPA. Thus, $L_{\mathrm{e}}(t) + L_{\mathrm{p}}(t) = 0$. Based on Eqs. (8) and (9), we have

$$V_{\mathrm{p}}(t) = \frac{\kappa_1 L_0}{\kappa_2} T(t). \tag{10}$$

Based on Eq. (10), the control voltage is proportional to the operating temperature and can be used to sense the temperature upon temperature compensation. Hence, acceleration and temperature are simultaneously measured.

Figure 4 shows the schematic of the FOFPA prototype system and the experimental setup. The light from the DFB laser (QDFBLD-1 550-10, Qphotonics, LLC), which is driven by a laser diode/temperature controller (ITC4001, Thorlabs), is coupled to the FOFPA via the fiber optic circulator. The reflected interference output from the FOFPA is detected and directly demodulated by the PD (2 053, New Focus) with a 30-fold attenuation of the DC output relative to the alternating current (AC) output. The PID controller, which is built in a real-time simulation system (DS1103 with MATLAB/Simulink, dSPACE GmbH), generates the control voltage for the PCUA to control the length change of the all-silica ILFFPE for active temperature compensation and measurement.

During the experiment, the FOFPA and matching mass are fixed on the two ends of an asbestos cement beam, which is mounted on a vibration exciter (4 809, B & K Corp.) via a calibrated piezoelectric accelerometer (PEA, 8 305, B & K Corp.). The end of the asbestos cement beam with the FOFPA is placed in an incubator to control the operating temperature. The measured acceleration is generated by a vibration exciter system composed of a sine random generator (1 207, B & K Corp.), a power amplifier (2 706, B & K Corp.), and a vibration exciter. The control voltage from the PID controller, the output from the PD, and the reference acceleration by the PEA system, which is composed of a PEA and a charge amplifier (0602, Lance), are displayed by a digital oscilloscope (TDS1002B, Tektronix).

Figure 5 shows the reflection spectrum of the FOFPA obtained using an optical sensing analyzer (si720, Micron Optics, USA). The visibility of the interference fringe of the FOFPA exceeds 8 dB. The cavity length of the all-silica ILFFPE obtained using the fringe counting method is approximately 4360 μm. If the wavelength of the DFB laser is set as 1557.35 nm using the laser diode/temperature controller, the FOFPA could be

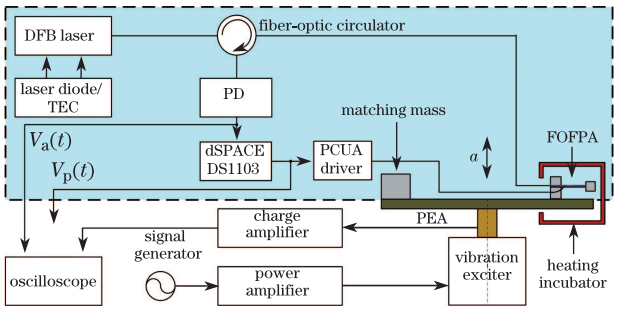

Fig. 4. Schematic of the FOFPA prototype system and experimental setup.

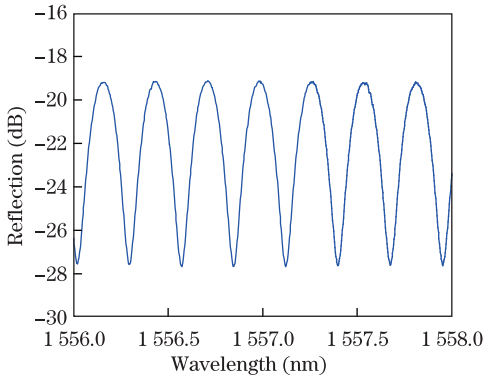

Fig. 5. Reflection spectrum of the FOFPA.

biased at the Q point. Figure 6 shows the relationship between the DC output of the interference output from the FOFPA and the control voltage with increasing from 0 to 10 V. Figure 6 shows that the DC output of the interference signal changes with increasing control voltage. The cavity length of the all-silica ILFFPE can then be controlled by driving the PCUA. Thus, the thermal strain of the cavity length of the all-silica ILFFPE can be compensated.

Figure 7 shows the time histories of the acceleration measured by the FOFPA system and the calibrated PEA under a 60-Hz sinusoidal vibration excitation at 25 °C. The acceleration measured by the FOFPA system is consistent with that by the calibrated PEA. Figure 8 shows the relationship between the acceleration measured by the FOFPA system and the calibrated PEA under a 60-Hz sinusoidal vibration excitation at 25 °C. The acceleration measured by the FOFPA system is linear to that by the calibrated PEA (see Fig. 8). The nonlinearity and the sensitivity of the output voltage and the measured acceleration are 0.93% and 0.826 V/g, respectively. The experimental result indicates the feasibility of the FOFPA system for acceleration measurement. Moreover, the frequency response of the FOFPA is measured at a frequency range from 10 to 1 000 Hz. The measured natural frequency is approximately 377 Hz, and the on-axis sensitivity is almost flat (10 to 200 Hz). In addition, to achieve temperature compensation, a low-pass filter with a cutoff frequency of 1 Hz is used to generate the DC output. Thus, the FOFPA can be operated at a frequency range from 1 to 200 Hz.

Figure 9 shows the variation in the control voltage of

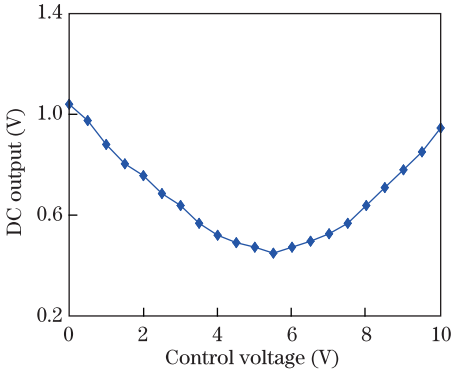

Fig. 6. Relationship between the DC output of the interference output from the cavity length of the all-silica ILFFPE and control voltage.

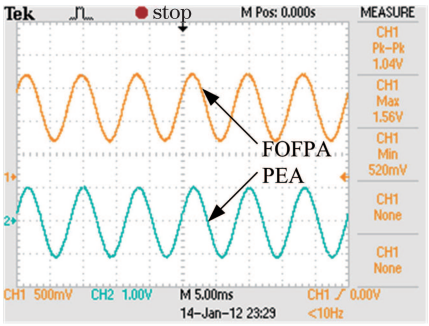

Fig. 7. Time histories of the acceleration measured by the FOFPA system and PEA.

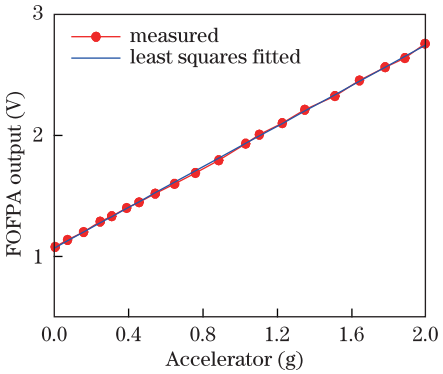

Fig. 8. Relationship between the amplitude of the output of the FOFPA system and acceleration measured by the PEA.

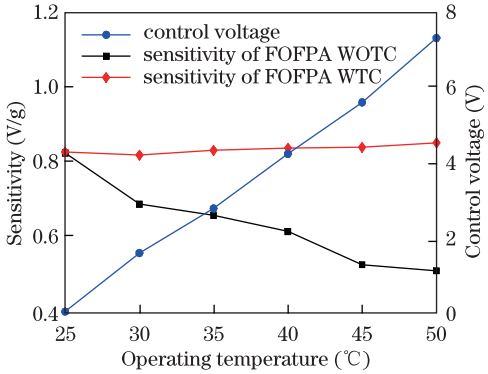

Fig. 9. Variation in the control voltage of the PCUA and sensitivity with increasing operating temperature.

the PCUA, the sensitivity of the FOFPA system with temperature compensation (WTC), and the sensitivity of the FOFPA system without temperature compensation (WOTC) with increasing operating temperature. Figure 9 shows that the sensitivity of the FOFPA system WOTC is very sensitive to the operating temperature even without considering the output waveform distortion caused by the change in the phase bias point. At a temperature range from 25 to 50 °C, the maximum deviation of sensitivity is more than 0.31 V/g, whereas that of the FOFPA system WTC is 0.025 V/g. We compared the sensitivity of the FOFPA system WTC and WOTC. The results show that the temperature dependency of the sensitivity of the FOFPA system can be effectively reduced and mostly eliminated. Moreover, the control voltage of the PCUA is proportional to the operating temperature with a nonlinearity of 1.75%.

In conclusion, a temperature-compensated FOFPA formed by symmetrically bonding an all-silica ILFFPE and a PCUA to two surfaces of a silica cantilever is presented. The all-silica ILFFPE senses the acceleration by translating the inertial force of the inertial mass generated by the acceleration into the cavity length change in the all-silica ILFFPE. The cavity length change is directly proportional to the phase shifts of interference output. To achieve temperature compensation and simultaneously measure acceleration and temperature, the cavity length of the all-silica ILFFPE is feedback controlled by the PCUA using the PID algorithm. The principle of the acceleration and temperature sensing of the FOFPA system is theoretically analyzed, and the FOFPA prototype system is fabricated and experimentally validated.

The results indicate that the fabricated FOFPA system can sense the acceleration and temperature with active temperature compensation. The nonlinearity of the output voltage of the FOFPA system to acceleration is less than 0.65%, and the nonlinearity of the control voltage to temperature is 1.75%. The maximum deviation of the sensitivity of the FOFPA system WTC at a temperature range from 25 to 50 °C is 0.025 V/g. In addition, the small thermal expansion of the all-silica cantilever could improve temperature compensation. However, the maximum compensated temperature cannot exceed the Curie temperature of the PCUA. Given that the DC component is used to compensate for the low-frequency temperature variation, the FOFPA could be applied in measuring non-low-frequency mechanical vibration.

This work was supported by the National Natural Science Foundation of China (No. 81127901), the Natural Science Foundation Project of CQ CSTC, Chongqing, China (No. 2009BA5072), and the Cultivation Fund of the Key Scientific and Technical Innovation Project, Ministry of Education of China (No. 708048).

References

1. G. Conforti, M. Brenci, A. Mencaglia, and A. G. Mignani, Appl. Opt. **28,** 5158 (1989).
2. A. Stefani, S. Andresen, W. Yuan, N. Herholdt-Rasmussen, and O. Bang, IEEE Photon. Technol. Lett. **24,** 763 (2012).
3. N. Basumallick, I. Chatterjee, P. Biswas, K. Dasgupta, and S. Bandyopadhyay, Sensors Actuators A Phys. **173,** 108 (2012).
4. J. Zhang, X. Qiao, M. Hu, Z. Feng, H. Gao, Y. Yang, and R. Zhou, Chin. Opt. Lett. **9,** 090606 (2011).
5. J. Zhang, X. Qiao, M. Hu, Z. Feng, H. Gao, Y. Yang, and R. Zhou, Chin. Opt. Lett. **9,** 090607 (2011).
6. Y. Weng, X. Qiao, Z. Feng, M. Hu, J. Zhang, and Y. Yang, Chin. Opt. Lett. **9,** 100604 (2011).
7. Y. Weng, X. Qiao, T. Guo, M. Hu, Z. Feng, R. Wang, and J. Zhang, IEEE Sens. J. **12,** 800 (2012).
8. N. Zeng, C. Shi, M. Zhang, L. Wang, Y. Liao, and S. Lai, Opt. Commun. **234,** 153 (2004).
9. R. D. Pechstedt and D. A. Jackson, Appl. Opt. **34,** 3009 (1995).
10. G. A. Cranch and P. J. Nash, J. Lightwave Technol. **18,** 1233 (2000).
11. C. Chen, D. Zhang, G. Ding, and Y. Cui, Appl. Opt. **38,** 628 (1999).
12. Y. Wang, H. Xiao, S. Zhang, F. Li, and Y. Liu, Meas. Sci. Technol. **18,** 1763 (2007).
13. G. Chen, X. Zhang, G. Brambilla, and T. P. Newson, Opt. Lett. **36,** 3669 (2011).
14. F. Peng, J. Yang , X. Li, Y. Yuan, B. Wu, A. Zhou, and L. Yuan, Opt. Lett. **36,** 2056 (2011).
15. F. Peng, J. Yang, B. Wu, Y. Yuan, X. Li, A. Zhou, and L. Yuan, Chin. Opt. Lett. **10,** 011201 (2012).
16. A. S. Gerges, T. P. Newson, J. D. C. Jones, and D. A. Jackson, Opt. Lett. **14,** 251 (1989).
17. Q. Lin, L. Chen, S. Li, and X. Wu, Meas. Sci. Technol. **22,** 015303 (2011).
18. J. M. Corres, J. Bravo, F. J. Arregui, and I. R. Matias, Sensors Actuators A Phys. **132,** 506 (2006).
19. T. Ke, T. Zhu, Y. Rao, and M. Deng, Microw. Opt. Technol. Lett. **52,** 2531 (2010).
20. Z. Zang and W. Yang, J. Appl. Phys. **109,** 103106 (2011).
21. Z. Zang, Opt. Commun. **285,** 521 (2012).
22. Z. Zang and Y. Zhang, J. Mod. Opt. **59,** 161(2012).
23. J. S. Sirkis, D. D. Brennan, M. A. Putman, T. A. Berkoff, A. D. Kersey, and E. J. Friebele, Opt. Lett. **18,** 1973 (1993).
24. J. Xu, X. Wang, K. L. Cooper, and A. Wang, Opt. Lett. **30,** 3269 (2005).
25. D. Wang, S. Wang, and P. Jia, Opt. Lett. **37,** 2046 (2012).
26. J. F. Dorighi, S. Krishnaswamy, and J. D. Achenbach, IEEE Trans. Ultrason. Ferroelectr. Freq. Control **42,** 820 (1995).
27. J. Chen, D. Chen, J. Geng, J. Li, H. Cai, and Z. Fang, Sensors Actuators A Phys. **148,** 376 (2008).
28. J. Chen, W. Li, H. Jiang, and Z. Li, Microw. Opt. Technol. Lett. **54,** 1668 (2012).
29. K. Bremer, E. Lewis, G. Leen, B. Moss, S. Lochmann, and I. A. R. Mueller, IEEE Sens. J. **12,** 133 (2012).